Available online at www.sciencedirect.com

ScienceDirect

Procedia Structural Integrity 2 (2016) 1085–1092

Structural Integrity Procedia

www.elsevier.com/locate/procedia

21st European Conference on Fracture, ECF21, 20-24 June 2016, Catania, Italy

Development of a probabilistic model for the prediction of fatigue life in the very high cycle fatigue (VHCF) range based on inclusion population

Anton Kolyshkin[a]*, Andrei Grigorescu[a], Edgar Kaufmann[b], Martina Zimmermann[c], Hans-Jürgen Christ[a]

[a]*Institut für Werkstofftechnik, Universität Siegen, Paul-Bonatz-Straße 9-11, Siegen 57068, Germany*
[b]*Department Mathematik, Universität Siegen, Walter-Flex-Straße 3, Siegen 57068, Germany*
[c]*Institut für Werkstoffwissenschaft, TU Dresden, Helmholtzstraße 7, Dresden 01062, Germany*

Abstract

The aim of the present work is to develop a statistical approach for the correlation between the quality of metallic materials with respect to the size and arrangement of inclusions and fatigue life in the VHCF regime by using the example of an austenitic stainless steel of type AISI 304 containing martensite from predeformation. For this purpose, the size and location of about 60000 inclusions in cross sections of an AISI 304 sheet in both longitudinal and transversal direction were measured and subsequently modeled using conventional statistical functions. This way a statistical model of inclusion population in AISI 304 was created. The model forms a basis for the subsequent statistical prediction of inclusion distribution in fatigue specimens and the corresponding fatigue lives. The size and location distributions of the crack initiating inclusions were defined based on the modeled inclusion population and the stress distribution in the fatigue specimen, using the probabilistic Monte Carlo framework. The experimentally obtained information about the correlation between the size and location of the crack initiating inclusions and corresponding fatigue lives allows an assessment of fatigue life of the specimens corresponding to the modeled crack initiating inclusions. Reasonable agreement was obtained between modeling and experimental results.

Keywords: austenitic stainless steel, AISI 304, inclusion distribution, very high cycle fatigue, fatigue life assessment

* Corresponding author. Tel.: +49 2717404627; fax: +49 2717402545
E-mail address: anton.kolyshkin@uni-siegen.de

Copyright © 2016 The Authors. Published by Elsevier B.V. This is an open access article under the CC BY-NC-ND license (http://creativecommons.org/licenses/by-nc-nd/4.0/).
Peer review under responsibility of the Scientific Committee of ECF21.
10.1016/j.prostr.2016.06.139

1. Introduction

Nomenclature

ΔK_I	stress intensity factor range (mode I)
σ_a	nominal stress amplitude
$\sigma_{a,l}$	local stress applied to an inclusion
$\sqrt{area}$	square root of the projection area of inclusion measured perpendicular to the applied load
N_f	number of cycles to failure
Y	geometry function
ν	inclusion aspect ratio

During the last two decades, numerous investigations in the area of very high cycle fatigue (VHCF) have shown that failures can occur even beyond the classical durability limit of $2 \cdot 10^6$ - 10^7 loading cycles (e. g. Müller-Bollenhagen et al. 2010, Murakami 2002). The failures are accompanied by a pronounced scatter regarding the number of cycles to failure and are caused by VHCF inherent damage mechanisms. Generally, the decrease of stress amplitude to the VHCF-relevant values entails the reduction of plastic deformation and consequently decreases the life fraction of the crack propagation period. So the crack initiation period extends and becomes more important for the fatigue life prediction in the VHCF range (Mughrabi 2006). On the basis of the crack initiation mechanisms in the VHCF range metallic materials were classified into two groups by Mughrabi. The first group includes pure (annealed) ductile materials and alloys containing no relevant intrinsic defects. The second group represents defect-afflicted materials that exhibit crack initiation at internal inclusions or pores in the VHCF range. The present paper is devoted to the investigation of the fatigue behaviour of the second material group.

In the VHCF range, the cyclic strength of metallic materials containing nonmetallic inclusions is predominantly determined by the properties of these defects (Li 2012). Inclusions arise during manufacturing processes and result in a localized distribution of plastic strain in isolated microstructural regions at VHCF-relevant stress amplitudes, and their presence and influence are hardly predictable analytically. Owing to the small size of the nonmetallic inclusions in modern clean steels amounting to no more than tens of microns (e. g. Müller-Bollenhagen et al. 2010) the current non-destructive analysis techniques are not able to reliably detect their presence in material structure (Beretta and Anderson 2002). Thus, the prediction of fatigue behaviour of a material containing randomly distributed microstructural defects can only be achieved using statistical methods accompanied by appropriate metallographic sampling strategies.

Several investigations showed that fatigue properties of a given material volume containing randomly distributed small defects while the material is subjected to uniformly distributed cyclic loads are related not to the average defect size but rather to the size of the maximum inclusion in the material volume (Murakami 2002, Beretta and Anderson 2002). On the basis of extreme value statistics Murakami and co-workers developed a rating method for clean steels based on the observation of the largest inclusions in a defined area. By means of this method the size of the maximum defect, which is assumed to be relevant for failure of a tested material volume, can be predicted. However, other investigations on fatigue behaviour of metallic defect-afflicted materials in the VHCF regime show that fatigue life also relates to the location of the failure-initiating defect (e. g. Li 2012). The present investigation is devoted to the development of a fatigue life prediction concept, which considers the size and location distribution of intrinsic defects as well as the acting damage mechanisms in the VHCF range.

2. Experimental setup and fatigue results

The fatigue tests were carried out on the metastable austenitic stainless steel AISI 304 with a high martensite volume fraction. The material was received in a sheet shape subjected to a solution annealing treatment. Hence, the texture effect on fatigue life was assumed to be negligible. In order to induce 60% martensite volume fraction in all fatigue specimens, metal strips of 14mm width were cut perpendicular to the rolling direction (RD, Fig. 1) and prestrained with a constant feed rate at the temperature of -90°C. The fatigue specimens were subsequently

machined by milling, grinded, mechanically and electrochemically polished. The specimen geometry in the highly stressed area is depicted in Fig. 2a.

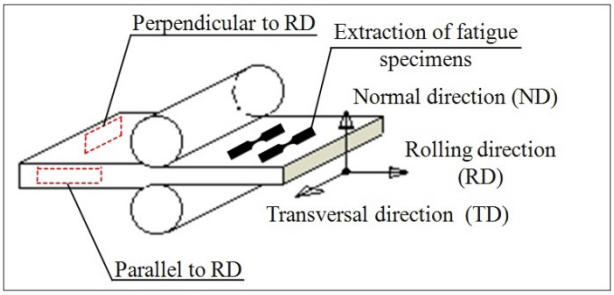

Fig. 1. Important planes and directions

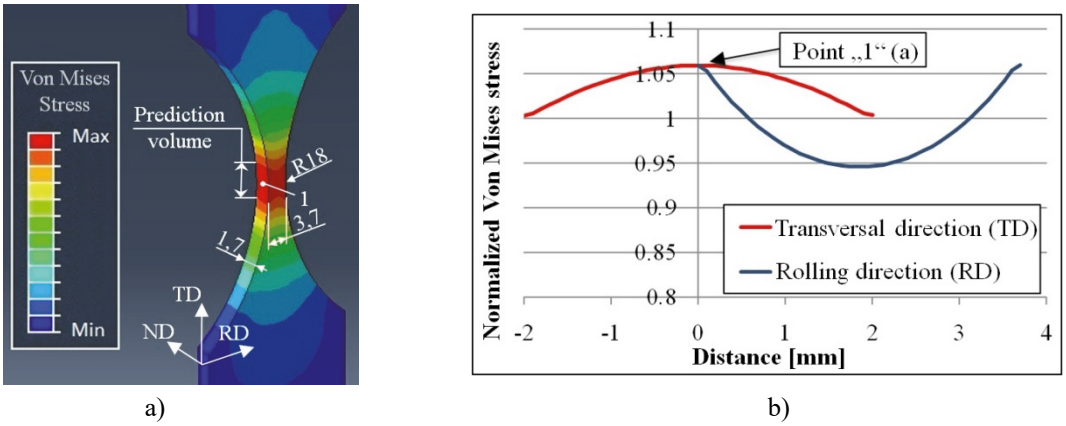

a) b)

Fig. 2. Von Mises stress distribution: a) in the fatigue specimen; b) in the center of the specimen along the RD and TD (see a)

Fatigue testing was executed by means of a resonant testing machine of type Testronic. The fatigue tests were carried out at laboratory air at room temperature under load control. At test frequencies of about 95 Hz undesirable heating of the specimens was avoided by active air cooling. All tests were executed under symmetrical push-pull condition (R= -1). After a decrease of the resonant frequency of 5 Hz, which roughly corresponds to 70% of specimen cross-section reduction caused by crack propagation, the fatigue tests were stopped. Subsequently, the fatigue samples were ruptured by applying a static tensile force in order to carry out fractographic analyses.

The S-N curve and the corresponding typical fracture surfaces are depicted in Fig. 3. The fatigue lives show a wide scatter of experimental results that extends over almost three decades of the S-N-curve. The fatigue results and the corresponding fracture surfaces can be divided into two groups. An example of the first group is depicted in Fig. 3b showing a scanning electron microscopy (SEM) photograph of a surface inclusion associated with fatal crack initiation in the HCF regime. The failures of the second specimen group in the VHCF range were caused by internal crack initiation at intrinsic inclusions accompanied by the formation of a fine granular area (FGA) and the VHCF typical "fish eye" morphology. All crack initiating inclusions have a disintegrated and elongated form with an average aspect ratio of $\nu = 10$. The specimens that actually failed in the VHCF range are situated very close to the chosen ultimate number of cycles of 10^8. Thus, the presented data can be used only for a limited representation of fatigue behaviour in the VHCF range.

Fig.4 shows the location of crack-initiating inclusions in the cross section of fatigue specimens failed at different stress amplitudes. At 510 MPa (Fig. 4a), about 50% of the inclusions are situated at the specimen surface and are related to a shorter fatigue life compared to the interior inclusions. At the stress amplitude of 490 MPa the amount of the interior crack initiating inclusions is higher and amounts to about 70%.

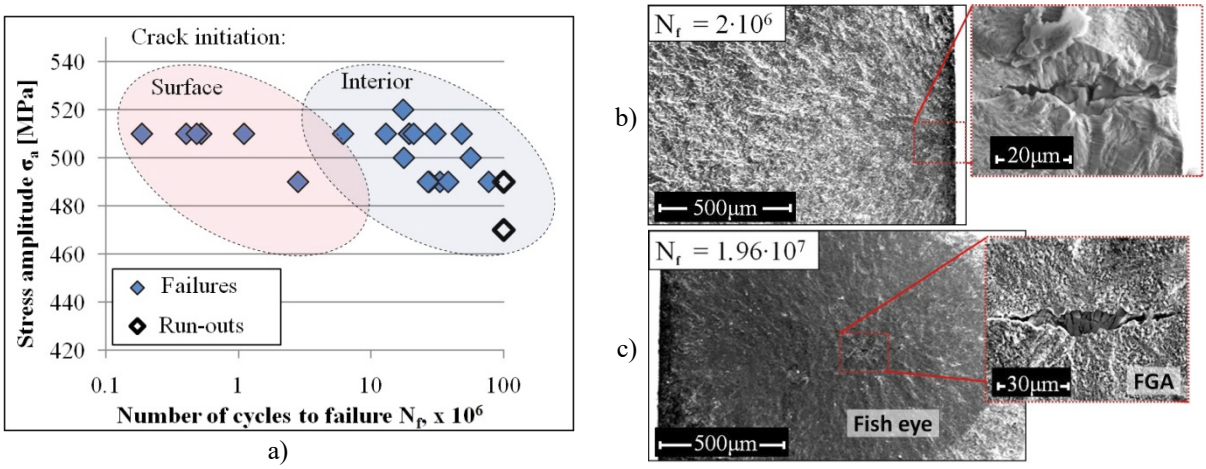

Fig. 3. a) S-N curve for AISI 304 with 60% martensite volume fraction; SEM photographs of the typical crack initiation b) at the surface and c) in the interior of a fatigue specimen

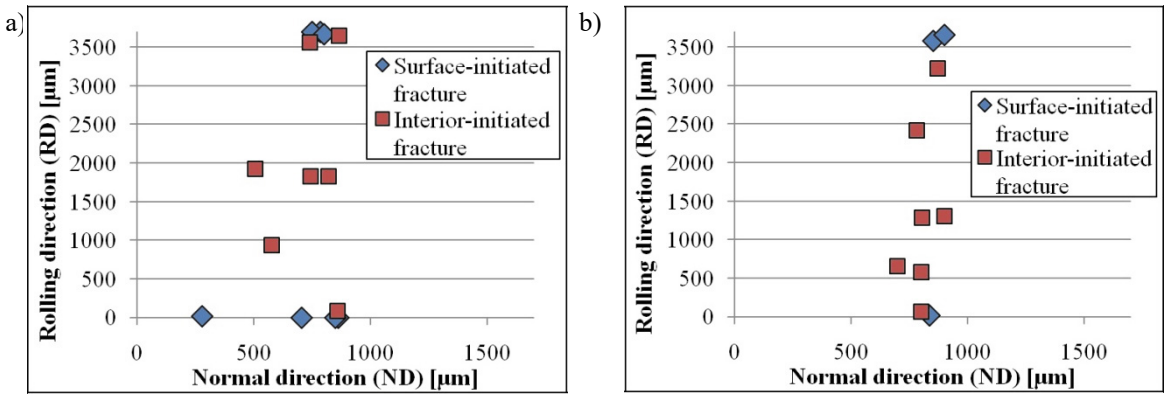

Fig. 4. Location of the crack initiating inclusions on the fracture surfaces of failed specimens that were tested at a) 510 MPa and b) 490 MPa.

The initial damage caused by single inclusions during the fatigue testing was assessed using the $\sqrt{area}$-concept which is based on a fracture-mechanics approach by Murakami (2002). According to this concept the stress intensity factor range (SIF, ΔK_I) for a fatigue crack originating at an inclusion can be calculated as follows

$$\Delta K_I = Y \cdot \sigma_{a,l} \cdot \sqrt{\pi \cdot \sqrt{area}} \tag{1}$$

Here Y is the geometry function which takes the value 0.5 for internal inclusions and 0.65 for surface inclusions. The calculation of SIF values for each failure-relevant inclusion detected on the fracture surfaces was carried out under consideration of the stress distribution caused by the specimen geometry (Fig. 2a). Depending on the location of inclusions the local stress amplitude $\sigma_{a,l}$ was calculated as the product of the nominal stress amplitude related to the minimum specimen cross section σ_a (Fig. 3a) and the "local" normalized stress presented in Fig. 2. The correlation between the calculated SIF values and corresponding fatigue lives is shown in Fig. 5a. A further subdivision of crack initiation at real surface inclusions and at near-surface inclusions revealed, that the SIF values that were calculated for crack-initiating surface inclusions as well as crack initiating inclusions situating in the vicinity of the specimen surface (if the distance to surface is smaller than the inclusion length, see Fig. 5b) show a clear correlation to the number of cycles to failure of fatigue specimens, which can be described by the power law. The different slopes of the plotted ΔK_I-N_f curves denote the difference in crack initiation mechanisms acting at the

specimen surface and in the specimen interior. The third group of markers in the presented ΔK_I-N_f diagram describes the failures that originated from inclusions situated deep below the specimen surface. Crack initiation at such inclusions leads to the additional "fish eye" formation (see Fig. 3c), which sufficiently increases the specimen fatigue life and shifts the calculated ΔK_I values form the defined ΔK_I-N_f dependence for the interior-induced fractures (red dashed line in Fig. 5a) to the right.

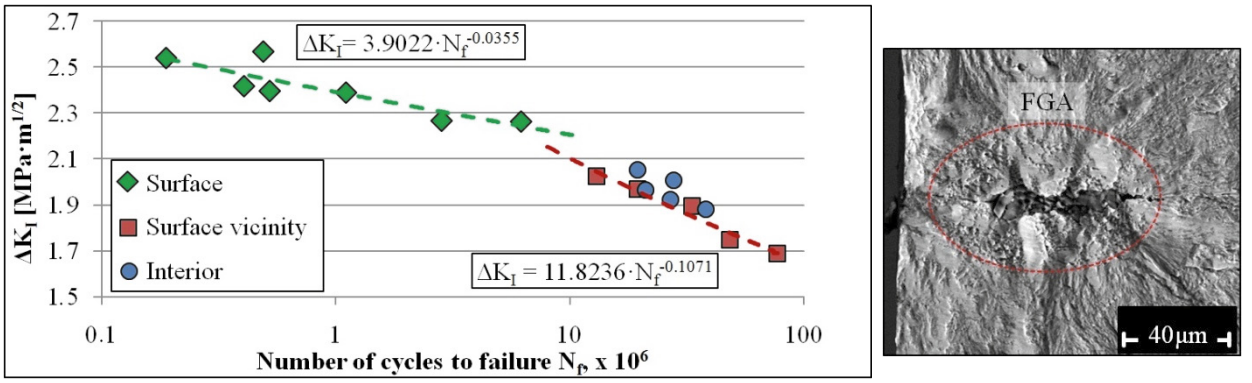

a) b)

Fig. 5. a) ΔK_I-N_f-curve for crack-initiating inclusions situated in different areas of the specimen cross section; b) initiating inclusion situated in the vicinity of the specimen surface

3. Creating a database for statistical fatigue life predictions

The database for statistical inferences about the fatigue behaviour of AISI 304 was created on the basis of metallographic observations on an overall number of 80 plane 2 x 14 mm sample cross sections. The samples were cut from a sheet of AISI 304 (here: fully austenitic condition) parallel and perpendicular to the rolling direction (Fig. 1), subsequently mechanically ground, polished and finally analysed by scanning the surface using a confocal 3D measuring laser microscope OLS4000 with a 100 magnification lens. Size and location of all inclusions in the obtained micrographs were defined by means of the image processing and analyzing software ImageJ. In order to express the 2-dimensional inclusion size, the parameter $\sqrt{area}$, which was measured on the sample surface, was used. Larger inclusions have the elongated and disintegrated shapes presented in Fig. 3b, 3c and 5b that presumably result from the hot rolling process and favor fatigue crack initiation.

Distributions of all measured inclusions along both RD and ND that are larger than fixed threshold sizes chosen to be 0 (all measured inclusions), 6 and 12 µm are presented in Fig. 6. While the inclusion distributions in RD and TD (not presented) do not show any explicit dependence on the threshold value and can be assumed to be uniform, the plots of relative frequencies relating to larger inclusions measured in ND illustrate the tendency of larger inclusions to concentrate in the centre of examined samples. Presumably, this phenomenon results from segregation processes during the ingot solidification progress (Akron Steel Treating Company) and is supported by the hot rolling process that is also responsible for the inclusion shape shown in Fig 3b, c and 5b.

It was assumed that failures originate at larger inclusions. Thus, only the size and location of larger inclusions exceeding some fixed size were modeled. The generalized Pareto distribution function (df) was proven by different authors (Li 2012, Shi et al. 1999) to be a reliable model for describing excesses of a random variable, such as size of the measured inclusions, above a given threshold value. The optimal threshold value for the presented data was chosen according to Shi et al. (1999) and assumed to be 12 µm. The generalized Pareto cumulative distribution function (cdf) is defined as

$$F(x \mid \lambda, k) = 1 - \left(1 - \frac{k(x - x_{\lim})}{\lambda}\right)^{\frac{1}{k}};\ x \geq x_{\lim} \tag{2}$$

with $x_{\lim}$ being the threshold value, $\lambda = 1.71$ being the scale parameter and $k = 0.0571$ being the shape parameter that were fitted to the measured inclusion size data exceeding the $x_{\lim}$ value.

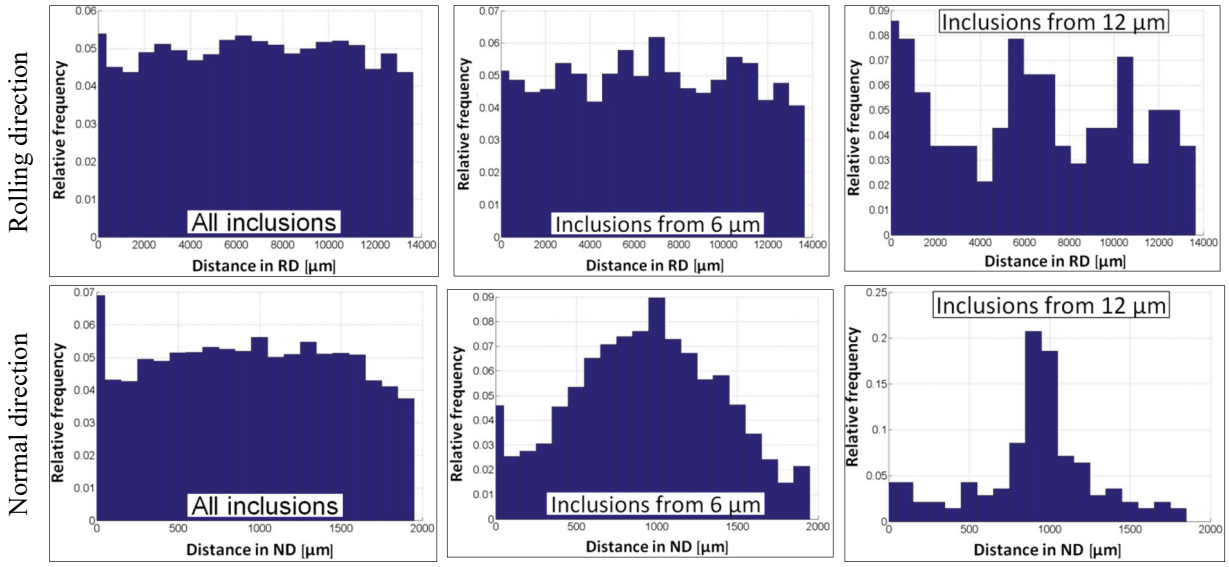

Fig. 6. Distribution of all measured inclusions along RD and ND (see Fig. 1,2)

In order to model the location of large inclusions exceeding the optimal threshold value (right column of Fig. 6) the uniform df for RD and TD as well as the Cauchy df for ND were selected. The Cauchy df enables to adequately describe the abrupt increase of the relative frequency of large inclusions from corners to the middle in ND and has a minimum mean square deviation from the measured data as compared to other distrubutions.

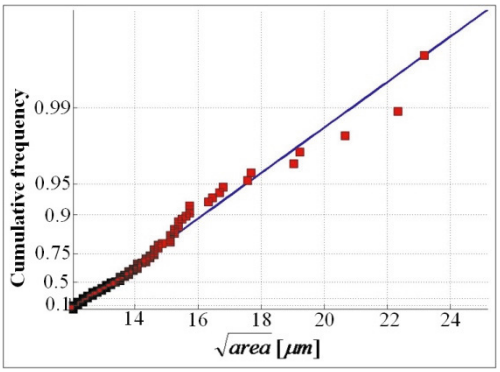

Fig. 7. Pareto probability plot of the inclusions exceeding the chosen threshold size value of 12 µm

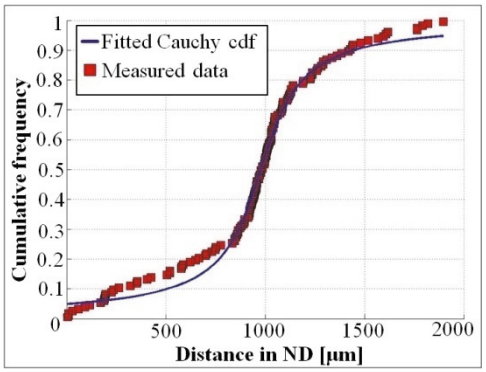

Fig. 8. Cumulative frequency of location of the inclusions exceeding the chosen 12 µm threshold size value along with the fitted Cauchy cdf

The Cauchy cdf is defined as

$$F(x \mid t,s) = \frac{1}{2} + \frac{1}{\pi} \cdot \arctan\left(\frac{x-t}{s}\right); -\infty < x < \infty \tag{3}$$

with the location parameter t and the scale parameter s being 978 and 153, respectively, for the measured inclusions exceeding the chosen 12 µm threshold size value. Fig.7 and 8 indicate the efficacy of the chosen Pareto and Cauchy dfs to describe the size and location distributions of the larger inclusions, respectively.

4. Modeling of the size and location distribution of initiating inclusions in fatigue specimens

It was assumed that interaction among inclusions is negligible (the inclusion fraction is lower than 0.1%) and failures can originate from all modeled inclusions.The modeling was performed in frames of probabilistic Monte Carlo simulations. Each simulation consisted of the following steps:

a) Generation of inclusion population within a defined prediction volume (Fig. 2a) corresponding to the measured inclusion density. The prediction volume was defined as the volume in the middle section of the fatigue specimen, in which the stress is at least 95% of the nominal stress in the specimen. This volume has a length of 3 mm (along the longitudinal axis of specimen) within which all failures appeared. The density of 3-dimensional inclusions within the prediction volume was defined on the basis of 2-dimensional inclusion measurements using the Woodhead analysis (Shi et al. 1999). The size and location of all inclusions in the prediction volume was modeled using eq. 2 and 3 in combination with uniform dfs, which describe the distribution of inclusions exceeding the chosen threshold size. The stress applied to each single inclusion was calculated by means of the linear interpolation of the stresses presented in Fig. 2.

b) Determination of geometry function Y for the modeled inclusions according to their location on the cross section of the prediction volume: If the $\nu \cdot \sqrt{area}\ / \pi$ value of the modeled inclusion is larger than its distance to the surface along the RD (Fig. 2a) or the $\sqrt{area}\ / \pi$ value is larger than the distance to the surface along the ND, then Y was assumed to be 0.5, otherwise Y equals 0.65.

c) Calculation of SIF for each modeled inclusion using the assigned size, location and value of the geometry function Y as well as the local stress in the inclusion surrounding volume (eq. 1).

d) Calculation of fatigue life N_f of the modeled prediction volume assuming that crack initiation starts simultaneously at all modeled inclusions. The fatigue life is calculated using the correlations presented in Fig. 5a as well as the defined values of Y-function.

e) The inclusion with minimum N_f among other modeled inclusions is assumed to be relevant to failure.

After 100 simulations at each of five stress amplitudes from 440 to 530 MPa the size and location of modeled failure-relevant inclusions were compared with experimental observations. Fig. 9 and 10a represent a reasonable agreement between simulation and experimental results (compare e.g. results for 490 MPa depicted in Fig. 4 and simulation results in Fig. 9b). Similarly to the experimental observations the modeled fatal-crack-initiating inclusions tend to concentrate in the middle of specimen along the ND and the number of surface-crack-initiating inclusions becomes larger with increasing stress amplitude (Fig. 9). The size distributions of the modeled and measured initiating inclusions have a similar slope and belong to the same statistical population in the Gumbel probability plot (Fig. 10a).

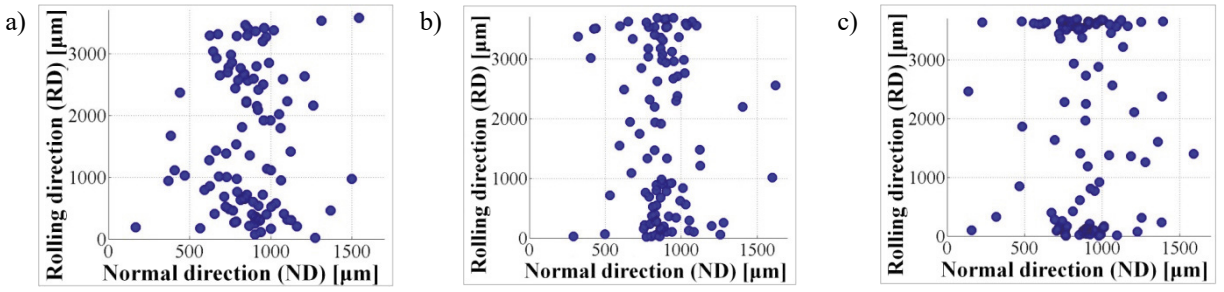

Fig. 9. Simulation results: location of failure-relevant inclusions simulated at a) 440, b) 490 and c) 530 MPa

5. Prediction of fatigue life

Since the influence of variance of inclusion size and location on fatigue life cannot be expressed explicitly, the confidence intervals for the tested steel were calculated on the basis of the executed simulations. The fatigue lives, which were obtained after 100 simulations at certain stress amplitudes, were arranged in ascending order. The values

of 10%, 50% (median) and 90% confidence band at each stress amplitude were assigned to the 10th, 50th and 90th value of modeled fatigue lives, respectively. The calculated confidence bands are plotted in Fig. 10b.

All fatigue results are situated within the calculated 10% and 90% confidence bands. Moreover, the simulation results correspond to the common statement that the scatter band widening in the VHCF range is a result of two simultaneously acting damage mechanisms. At moderate stress amplitudes, when only crack initiation at interior inclusions appears, the scattering decreases (see e. g. Lee 2012).

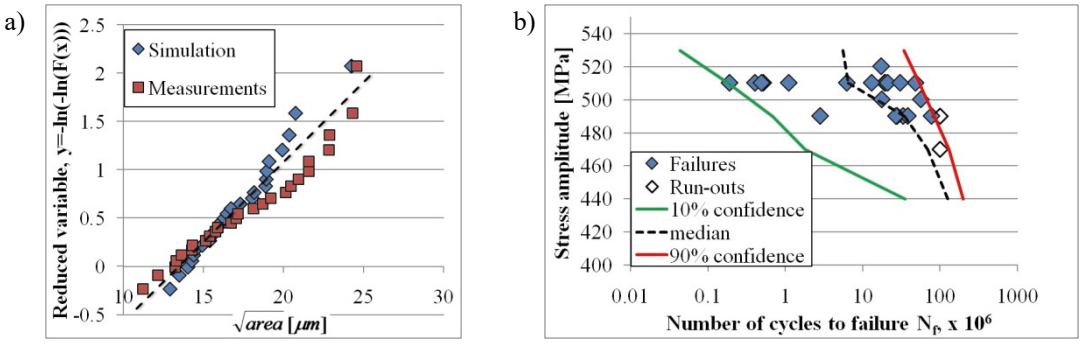

Fig. 10. Simulation results: a) size of simulated and measured failure-relevant inclusions in the Gumbel probability plot; b) S-N curve with calculated confidence bands

6. Summary

The present study describes the application of conventional statistical functions and methods, which can simulate failure-relevant microstructural defects and, hence, reduce the number of fatigue tests required for the fatigue life prediction in the VHCF range. In order to describe the size and location of inclusions exceeding the chosen threshold size the Pareto and Cauchy dfs as well as uniform dfs were used. On the basis of these dfs an inclusion population model was formed, which was used together with the calculated stress distribution in order to predict the size and location of initiating inclusions. The experimentally obtained information about the correlation between the size and location of the crack-initiating inclusions and corresponding fatigue lives allows an assessment of life of the fatigue-tested specimens corresponding to the modeled initiating inclusions. On the basis of the simulation results the fatigue life of the tested metastable austenitic steel AISI 304 with a martensite volume fraction of 60% as well as its uncertainty was modeled. The modeled fatigue behaviour shows a reasonable agreement with the experimental data.

Acknowledgements

This work was financially supported by the Deutsche Forschungsgemeinschaft, CH 92/46-1

References

Akron Steel Treating Company. Modern Steels and their Properties, reference book, information on http://www.akronsteeltreating.com.

Beretta, S., Anderson C., 2002.Extreme Value Statistics in Metal Fatigue, Societ‘aItaliana di Statistica, Attidella XLI RiunioneScientifica, 251–260.

Li, S. X., 2012. Effects of Inclusions on Very High Cycle Fatigue Properties of High Strength Steels, International Materials Reviews 57, 92-114.

Mughrabi, H., 2006. Specific Features and Mechanisms of Fatigue in the Ultrahigh-Cycle Regime. International Journal of Fatigue 28, 1501-1508.

Müller-Bollenhagen, C., Zimmermann, M., Christ, H.-J., 2010. Very High Cycle Fatigue Behaviour of Austenitic Stainless Steel and the Effect of Strain-Induced Martensite. International Journal of Fatigue 32, 936-942.

Murakami,Y., 2002. Metal Fatigue: Effects of Small Defects and Nonmetallic Inclusions, Elsevier, Oxford.

Shi, G., Atkinson, H.V., Cellars, C.M., Anderson, C.W., 1999. Application of the Generalized Pareto Distribution to the Estimation of the Size of the Maximum Inclusion in Clean Steels. Acta Materialia 47, 1455-1468.